RESEARCH

Low frequency-to-intensity noise conversion in a pulsed laser cavity locking by exploiting carrier envelope offset

Francesco Canella[1,2] · Edoardo Suerra[2,3] · Dario Giannotti[2] · Gianluca Galzerano[2,4] · Simone Cialdi[2,3]

Abstract

We report on the dependence of the frequency-to-intensity noise conversion in the locking of an ultrafast laser against a high-finesse optical enhancement resonator from the carrier envelope offset frequency. By a proper combination of the cavity finesse and laser carrier envelope offset frequency, it is possible to optimize the signal-to-noise ratio of the laser intensity trapped into the optical resonator. In this paper, we describe the effect of the laser-enhancement cavity coupling on the intracavity power relative noise, and we demonstrate both theoretically and experimentally its reduction.

1 Introduction

Frequency-to-intensity noise conversion in the laser stabilization with respect to high-finesse optical resonator is a well known problem [1–3] and over the years several experimental solutions have been implemented to reduce the intensity noise of the cavity trapped radiation: the use of noise-immune high-frequency modulation detection schemes [3], by means of wide control loop bandwidths in the frequency locking schemes [4], and using cavity ring-down methods [5, 6]. In the majority of the investigated cases, the laser sources operated in a continuous wave regime. However, in the last 20 years thanks to the introduction of the optical frequency comb sources, the locking of ultrafast broadband laser sources to high-finesse resonators is of extreme interest in a wide variety of sensing/spectroscopic applications [7–9] as well as in extreme non-linear optics for the generation of coherent radiation in the UV and XUV spectral regions [10–12]. In spectroscopic applications, cavity locking is used to increase by several orders of magnitude the interaction

length with the samples, while in UV and XUV generation, it can be exploited to increase the circulating laser intensity. In any case, low intensity noise of the trapped laser field is a mandatory requirement to obtain the highest signal-to-noise ratio (SNR) and temporal coherence [7, 8, 10–12].

In this paper, we demonstrate a novel solution to reduce the residual frequency-to-intensity noise conversion when a pulsed laser is coupled to a high-finesse enhancement resonator. This is related to the use of slightly detuned resonance conditions between the cavity resonances and laser modes by acting on the Carrier Envelope Offset (CEO) frequency of the pulsed laser source. In this way, the modes of the laser comb that are far from the spectrum center, and the ones that are near the spectrum center give contributions to the second order derivative of the frequency-to-intensity fluctuation function with opposite signs. For this reason, the contributions of these different regions of the laser spectrum compensate each other. By a proper combination of the CEO frequency detuning and cavity finesse values, large cavity gain factor can be obtained together with a strong reduction of the frequency-to-intensity noise conversion, an essential requirement for the generation of X-ray radiation by inverse Compton scattering (ICS) [13] with low-intensity noise. After the theoretical description of the method, a detailed experimental characterization of the technique is performed using a mode-locked Yb:fiber laser at 1035 nm, and a ring cavity optical resonator. With a gain factor as large as 1130, we demonstrated an integrated frequency to intensity noise conversion reduced from 8% to less than 0.5%.

The paper is structured in four sections. The principles and the theoretical treatment of the method is presented in

✉ Francesco Canella
francesco.canella@polimi.it

1   Dipartimento di Fisica, Politecnico di Milano, Piazza Leonardo da Vinci 32, 20133 Milan, Italy

2   Istituto Nazionale di Fisica Nucleare, Sezione di Milano, via Celoria 16, 20133 Milan, Italy

3   Dipartimento di Fisica, Università degli Studi di Milano, Via Celoria 16, 20133 Milan, Italy

4   Istituto di Fotonica e Nanotecnologie-CNR, Piazza Leonardo da Vinci 32, 20133 Milan, Italy

Sect. 2, whereas the numerical simulation are reported in Sect. 3. Section 4 shows the experimental characterization of the method. Finally, Sect. 5 closes the paper with some concluding remarks.

2 Theory

The link between the CEO frequency f_{ceo} and the frequency-to-noise conversion in an optical cavity can be shown starting from the time-domain electric field of a mode-locked laser. The train of pulses in time domain is given by the superposition of the field of several modes oscillating in phase. If every mode has a frequency ν_m, being $m \in \mathbb{N}$, the electric field $\mathscr{E}(t)$ can be written as:

$$\mathscr{E}(t) = \sum_{m=0}^{\infty} \sqrt{S_m}\, e^{-i2\pi \nu_m t + i\varphi_m(t)} \tag{1}$$

where S_m is the laser power spectrum $S(\nu)$ evaluated at the frequency ν_m, while φ_m is a generic phase noise. Typically, φ_m contains both slow components (essentially related to mechanical vibrations), and fast components. In the spectral domain, Eq. (1) becomes:

$$E(\nu) = \mathfrak{F}[\mathscr{E}(t)] = \sum_{m=0}^{\infty} \sqrt{S_m} \int e^{i2\pi(\nu - \nu_m)t} e^{i\varphi_m(t)}\, \mathrm{d}t \tag{2}$$

where $\mathfrak{F}[\cdot]$ denotes the Fourier transform. When the optical bandwidth of the comb is much narrower than the carrier ν_0, we assume that the noise $\varphi_m(t) = \varphi(t)$ is equal for all the laser teeth.

Furthermore, we assume that $\varphi(t) \ll 2\pi$, so that we can expand the exponential to first order, leading to

$$\begin{aligned} E(\nu) &= \sum_{m=0}^{\infty} \sqrt{S_m} \int e^{i2\pi(\nu-\nu_m)t}(1 + i\,\varphi(t))\, \mathrm{d}t \\ &= \sum_{m=0}^{\infty} \sqrt{S_m}\big(\delta(\nu - \nu_m) + i\,\phi(\nu - \nu_m)\big) \equiv \sum_{m=0}^{\infty} E_m(\nu) \end{aligned} \tag{3}$$

Equation (3) tells us that the laser spectrum has a comb-like structure of Dirac deltas, broadened by the noise $\phi(\nu) = \mathfrak{F}[\varphi(t)]$. Thus, the laser power is given by

$$\begin{aligned} P^{(laser)} &= \sum_{m=0}^{\infty} S_m \big|\delta(\nu - \nu_m) + i\,\phi(\nu - \nu_m)\big|^2 \\ &= \sum_{m=0}^{\infty} S_m \Phi_m \equiv \sum_{m=0}^{\infty} P_m^{(laser)} \end{aligned} \tag{4}$$

where $\Phi_m = \big|\delta(\nu - \nu_m) + i\,\phi(\nu - \nu_m)\big|^2$.

Note that in Eq. (4), the crossed products cancel since different modes do not overlap.

To complete the discussion about the laser, we also remind that the frequencies of its modes are [14, 15]:

$$\nu_m^{(laser)} = m f_{rep} + \frac{\Delta\phi_{cep}}{2\pi} f_{rep} = m f_{rep} + f_{ceo} \tag{5}$$

where f_{rep} is the separation of the teeth corresponding to the repetition rate of the laser, while $\Delta\phi_{cep}$ is its Carrier-Envelope Phase shift, generated by the different phase and group velocities in the laser cavity. The so-called Carrier-Envelope Offset frequency is defined as $f_{ceo} = \frac{\Delta\phi_{cep}}{2\pi} f_{rep}$.

The laser pulses can be coupled to an optical enhancement cavity [16] to stack them and increase their power with a passive gain proportional to the resonator finesse. In particular, for an overcoupled cavity of finesse F, the maximum achievable gain is $\frac{2}{\pi}F$. The spatial modal structure of an enhancement cavity is given by the well-known Hermite–Gaussian polynomial [17], when operating in an ideal case (vacuum environment and no dispersion). However, if we consider dispersion, the circulating laser pulses acquire a phase depending on the resonator mirrors and air dispersion, which adds to the Guoy phase related to the non-planar nature of the resonating field. Such additional phase must be taken into account in a more realistic and general discussion [18]. In this case, the resonance condition for the fundamental cavity spatial modes TEM$_{00}$ is given by:

$$kL - 2\phi_G + \phi_M(\nu) + \phi_A(\nu) = 2\pi n \tag{6}$$

where ϕ_G is the Gouy phase, L is the cavity length (we assume here a ring resonator), $k = 2\pi\nu/c$ is the wave vector, while $\phi_M(\nu)$ and $\phi_A(\nu)$ are the frequency-dependent phases introduced by the cavity mirrors reflections and air, respectively. Notice that the Gouy phase for an astigmatic enhancement cavity, as in our case, is obtained by the sum of two different contributions, depending on the cavity geometry on the horizontal and vertical directions: $\phi_G = \phi_{G,x}/2 + \phi_{G,y}/2$.

The phases ϕ_G, ϕ_M and ϕ_A can be collected in one general term $\phi_{cav}(\nu)$. This can be expanded around ν_0 as $\phi_{cav} = \phi_{cav,0} + \nu\,\phi'_{cav,0} + \delta\phi_{cav}(\nu)$, with $\delta\phi_{cav}$ containing only second-and higher order terms in ν [19]. From Eq. (6) it is possible to obtain a general expression for the enhancement cavity longitudinal modes:

$$\nu_n^{(cav)} = \frac{c}{L\left(1 + \frac{c}{2\pi L}\phi'_{cav,0}\right)}\left(n - \frac{\phi_{cav,0}}{2\pi} - \frac{\phi'_{cav,0}}{2\pi} - \frac{\delta\phi_{cav}(\nu)}{2\pi}\right) \tag{7}$$

The effect of the quadratic term $\delta\phi_{cav}$ is to prevent a perfect uniformity of cavity mode spacing. On the other hand, it can be neglected in case of small input laser spectra and small enhancement cavity Finesse values. This is the case of our experimental setup, where we specifically
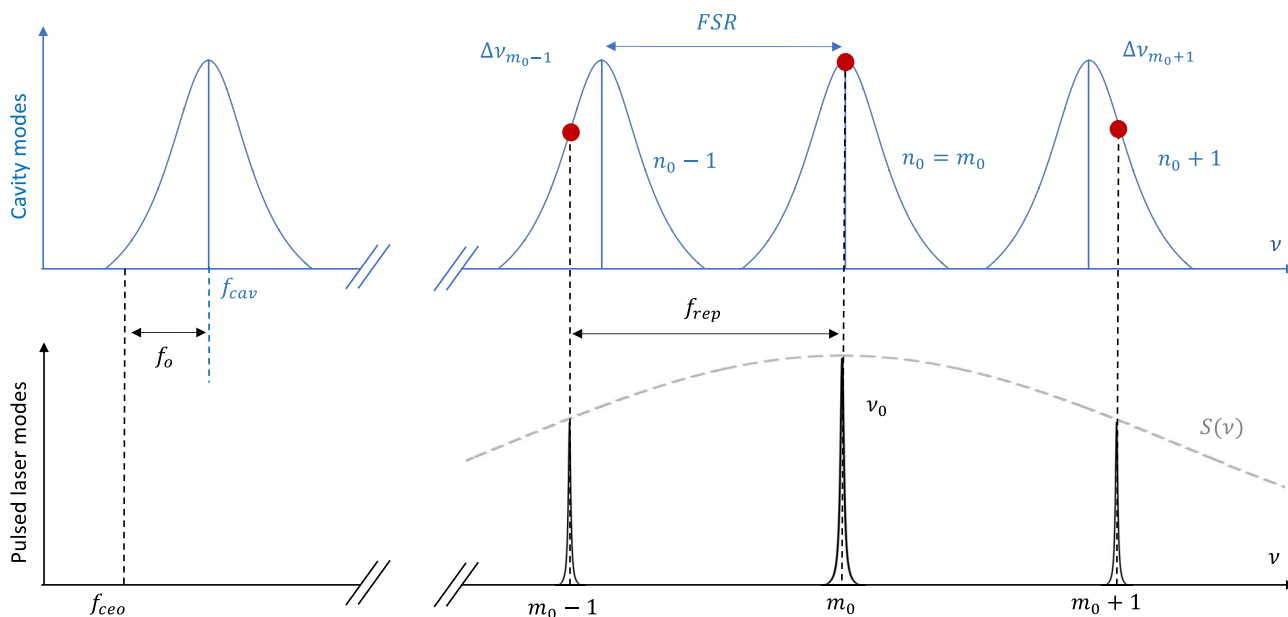
Fig. 1 Laser and cavity modes in frequency domain. In this representation, the cavity is stabilized to the laser on the tooth $n_0 = m_0$ with the PDH technique. The teeth with indexes $n \neq m_0$ have a detuning $\Delta\nu_m$, which is positive for $m > m_0$ or negative for $m > m_0$. In this scheme $f_{cav} > f_{ceo}$, so $f_0 < 0$

chose to couple a 2.7 nm input spectrum with a cavity of Finesse < 5000.

The first term of Eq. (7) is the Free Spectral Range $\text{FSR} = c \left[L \left(1 + \frac{c}{2\pi L} \phi'_{cav,0} \right) \right]^{-1}$ of the enhancement cavity, while, after neglecting $\delta\phi_{cav}$, all the terms in the bracket are constant, except for the longitudinal index n, so they can be collected in a single constant term k_{cav}. Now, defining $f_{cav} = \text{FSR} \cdot k_{cav}$, the expression of the enhancement cavity fundamental spatial modes TEM_{00} reduces to

$$\nu_n^{(cav)} = n\,\text{FSR} + f_{cav}. \tag{8}$$

Hence, similar to the laser comb mode spectrum, even the modal structure of the enhancement cavity presents an offset frequency, f_{cav}. The highest passive gain is achieved when the laser and the enhancement cavity teeth are perfectly matched. This condition can be obtained and maintained during time exploiting the well known Pound-Drever-Hall (PDH) technique [20], which, in our case, stabilizes the FSR of the cavity to match the laser teeth. If we set m_0 to be the laser spectrum barycenter, so that once the enhancement cavity is locked the PDH signal is 0, the maximum coupling between the combs is obtained by stabilizing the laser tooth m_0 to the cavity tooth n_0, with $n_0 = m_0$. Starting from Eqs. (5) and (8), and taking this last condition $n_0 = m_0$, we can write the following general resonance condition

$$\nu_{m_0}^{(laser)} = \nu_{m_0}^{(cav)} \quad \Rightarrow \quad m_0 f_{rep} + f_0 = m_0\,\text{FSR}$$

where $f_0 = f_{ceo} - f_{cav}$ is the relative frequency offset between laser and cavity combs. The PDH technique fixes the FSR of the cavity to $\text{FSR} = f_{rep} + \frac{f_0}{m_0}$. A clear representation of the two combs coupling is reported in Fig. 1. A perfect overlap of the cavity and the laser modes is possible only if $f_0 = 0$, otherwise, each tooth has a detuning given by

$$\Delta\nu_m(f_0) = \frac{f_0}{m_0} \Delta m, \tag{9}$$

where $\Delta m = m - m_0$. When the laser-cavity locking condition is achieved, only relative detunings are relevant. Thus, it is equivalent to introduce noise from the laser or the cavity, and from now on we attribute all the noise to the laser without loss of generality. On the other hand, the same results can be achieved by assuming $\varphi(t) = 0$, while introducing a noise $\delta\text{FSR}(t)$ on the cavity frequencies.

Now, we study how f_0 affects the laser-cavity coupling, hence the intracavity power and its noise. We start from considering the total intracavity power in relation with the incoming laser power and the cavity response:

$$\begin{aligned} \text{P}^{(cav)}(f_0) &= \sum_{m=0}^{\infty} P_m^{(laser)} \frac{1 - R_1}{1 + R - 2\sqrt{R}\cos\frac{2\pi\Delta\nu_m(f_0)}{\text{FSR}}} \\ &= \sum_{m=0}^{\infty} P_m^{(laser)} \Gamma\left(\Delta\nu_m(f_0)\right) \equiv \sum_{m=0}^{\infty} P_m^{(cav)}\left(\Delta\nu_m(f_0)\right) \end{aligned} \tag{10}$$

where $\Gamma\big(\Delta\nu_m(f_0)\big)$ is the gain of the cavity for the mode m detuned by $\Delta\nu_m(f_0)$, R_1 is the input cavity mirror power reflectivity, and R the product of all the cavity mirrors' reflectivity. Notice that we explicated the dependence of $\Delta\nu_m$ on f_0, following Eq. (9). The total cavity gain Γ_{tot} is then given by the weighted average of the single modes gains over all the coupled modes. In terms of power, assuming an incoming radiation power $\mathrm{P}^{(\text{laser})}$, the stored power is simply given by $\mathrm{P}^{(\text{cav})} = \mathrm{P}^{(\text{laser})} \cdot \Gamma_{\text{tot}}$.

$$\Gamma_{\text{tot}} = \frac{\sum_m P_m^{(\text{cav})}\big(\Delta\nu_m\big)}{\sum_m P_m^{(\text{laser})}} \tag{11}$$

While Γ_{tot} is not directly accessible, the transmitted power is, and it is directly proportional to the gain as $\mathrm{P}^{(\text{trans})} = \big(1 - R_2\big)\mathrm{P}^{(\text{laser})}\Gamma_{\text{tot}}$. In the latter equation, R_2 is the reflectivity of the mirror used to detect the cavity transmission.

As far as the peak power of the intracavity pulses P_{peak} is concerned, we find an implicit dependence on f_0 hidden in the coupling with the cavity. Indeed, the cavity acts as a filter for the laser, both in amplitude and in phase. The additional phase experienced by each mode, which impacts on the temporal structure of the pulses, must be taken into account to properly estimate P_{peak}. As f_0 increases, both the cavity spectral filtering effect and the phase become more and more important, broadening in time the stored pulses and lowering P_{peak}. We can write

$$\mathrm{P}_{\text{peak}} = \max\left\{\left|\mathfrak{F}^{-1}\left[\sqrt{S(\nu)}\,F_{\text{cav}}(\nu)\,e^{i\phi_{\text{cav}}(\nu)}\right]\right|^2\right\} \tag{12}$$

where F_{cav} and ϕ_{cav} are the cavity filter function in amplitude and phase. In experimental setups, there is often an additional detuning f_{pdh}, given by an electronic offset in the PDH stabilization, which locks the enhancement cavity mode n_0 not exactly on the central frequency of the correspondent laser mode m_0. The PDH stabilization offset can be included in the theory by simply considering $\Delta\nu_m = \left(\frac{f_0}{m_0}\right)\Delta m + f_{\text{pdh}}$.

At this point, we are able to debate on a particularly interesting and important issue: the noise transfer from the laser and the cavity to the stored power in the coupled system. There are essentially two noise sources for the stored power: the laser intensity noise and the frequency noise. Intensity noise is substantially due to power fluctuations of the laser source, and we will not cover it in this work. On the contrary, frequency noise induces fluctuations in the stored power, because it causes time-dependent additional detuning $\delta f(t)$. This frequency noise is strictly dependent on the phase noise, indeed $\delta f(t) = (2\pi)^{-1}\mathrm{d}\varphi(t)/\mathrm{d}t$. Usually, it can be associated to a $\delta f(\nu)$ and a spectral distribution with a standard deviation $\sigma_{\delta f}$. The introduction of $\sigma_{\delta f}$ is quite important, because this is a parameter directly accessible

from the experimental setup, by measuring the integrated frequency noise discriminated by the cavity while the locking with the laser is maintained [21]. To study the influence of δf on the power fluctuations, the function $\Gamma\big(\Delta\nu_m + \delta f\big)$ can be expanded around the offset detuning frequency $\Delta\nu_m$ as

$$\begin{aligned}\Gamma\big(\Delta\nu_m + \delta f\big) &\approx \Gamma\big(\Delta\nu_m\big) \\ &+ \left.\frac{\mathrm{d}\Gamma}{\mathrm{d}\nu}\right|_{\Delta\nu_m}\delta f + \frac{1}{2}\left.\frac{\mathrm{d}^2\Gamma}{\mathrm{d}\nu^2}\right|_{\Delta\nu_m}\delta f^2.\end{aligned} \tag{13}$$

Therefore, recalling that the total cavity gain is the average gain of the teeth, weighed on the coupled laser spectrum $S(\nu)$, and the same holds for the fluctuations, we separate the gain in two components Γ_{tot} and $\delta\Gamma_{\text{tot}}$, respectively, writable as

$$\begin{aligned}\Gamma_{\text{tot}} &= \frac{\sum_m S_m\Gamma\big(\Delta\nu_m + \delta f\big)}{\sum_m S_m} \approx \frac{\sum_m S_m\Gamma\big(\Delta\nu_m\big)}{\sum_m S_m} \\ &= \frac{1}{N}\sum_m S_m\Gamma\big(\Delta\nu_m\big)\end{aligned} \tag{14}$$

$$\begin{aligned}\delta\Gamma_{\text{tot}}(\delta f) &= \frac{1}{N}\sum_m S_m\big[\Gamma\big(\Delta\nu_m + \delta f\big) - \Gamma\big(\Delta\nu_m\big)\big] \\ &= \frac{1}{N}\left(\sum_m S_m\left.\frac{\mathrm{d}\Gamma}{\mathrm{d}\nu}\right|_{\Delta\nu_m}\delta f + \frac{1}{2}\sum_m S_m\left.\frac{\mathrm{d}^2\Gamma}{\mathrm{d}\nu^2}\right|_{\Delta\nu_m}\delta f^2\right)\end{aligned} \tag{15}$$

Γ_{tot} in Eq. (14) is noise-immune, and it is only an implicit function of the system offset f_0 and of the eventual f_{pdh}. We also defined $N \equiv \sum_m S_m$ to simplify the notation on the latter equations. The first term of Eq. (15) is an odd function when $f_{\text{pdh}} = 0$, thus the sum over all the modes around m_0 vanishes, because $\Delta\nu_m < 0$ or $\Delta\nu_m > 0$ for $m < m_0$ or $m > m_0$, respectively. Hence $\left.\frac{\mathrm{d}\Gamma}{\mathrm{d}\nu}\right|_{\Delta\nu_m} < 0$ or $\left.\frac{\mathrm{d}\Gamma}{\mathrm{d}\nu}\right|_{\Delta\nu_m} > 0$. Notice that in principle f_{pdh} can differ from zero, and this would induce a symmetry break that causes a non-negligible noise arising from first-order terms. On the other hand, f_{pdh} can be easily set to zero by adjusting the feedback parameters. The second term is the most important for us, because it can be adjusted by manipulating the offset f_0 (hence f_{ceo}) to reduce the noise transfer.

In Fig. 2, a representation of the noise transfer reduction via f_0 principle is given. Since the second-order derivative of Γ is an even function, it assumes both positive and negative values at increasing detuning. In particular, when $f_0 = 0$, the term $\left.\frac{\mathrm{d}^2\Gamma}{\mathrm{d}\nu^2}\right|_{\Delta\nu_m}$ is negative for all the comb teeth. For this reason, the second-order contributions to the noise sum together, because they are all concordant. On the other hand, when the offset f_0 is non-zero, the modes different from m_0 experience a detuning proportional to Δm, as written above. Hence, if f_0 becomes larger enough, the detuning
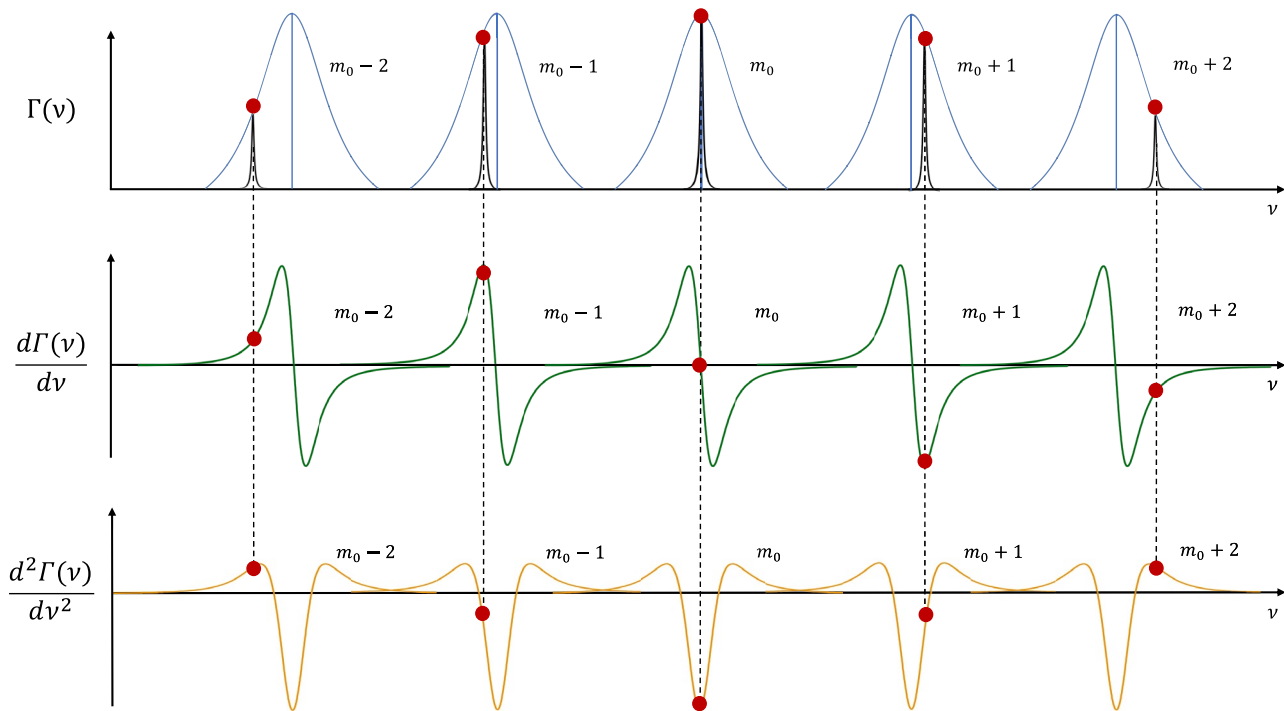
Fig. 2 Representation of the effect of f_0 on the evaluation point of the cavity gain and its derivatives (from above to below: Γ with the laser teeth, $d\Gamma/d\nu$, and $d^2\Gamma/d\nu^2$ as functions of ν). At increasing offset, the gain progressively decreases with the distance from the central mode m_0. The first derivative terms on the right balance the ones on the left, since $d\Gamma/d\nu$ is an even function (when $f_{\text{pdh}} = 0$). On the other hand, $d^2\Gamma/d\nu^2$ is odd. Thus, the central modes contributions are compensated by the external modes, where the second-order derivative becomes positive

of the most external modes is sufficient to contribute with positive $\frac{d^2\Gamma}{d\nu^2}\big|_{\Delta\nu_m}$. In this situation, the modes close to m_0 give quadratic noise contributions with opposite sign with respect to the external ones ($\frac{d^2\Gamma}{d\nu^2}\big|_{\Delta\nu_m} < 0$ and $\frac{d^2\Gamma}{d\nu^2}\big|_{\Delta\nu_m} > 0$, respectively). The resulting total noise is then reduced with respect to the $f_0 = 0$ case, since now part of the contributions cancel out. Increasing f_0, this second-order cancellation becomes more efficient. However, as a drawback, increasing f_0 results in a decrease of Γ_{tot}. For this reason, it is important to compare the noise suppression with the cavity passive gain loss, at a given offset f_0. As we will show in the next sections, the noise suppression is more effective than the gain drop, and, consequently, it is possible to dramatically reduce the intensity noise without a large decrease in the stored power. A last step useful to understand the impact of noise suppression is to evaluate how a frequency noise $\sigma_{\delta f}$ affects the integrated noise σ_P of the intracavity power. This is directly given by the fluctuation of the gain Γ_{tot}, namely σ_Γ. To simplify the notation, we define $\alpha \equiv \frac{1}{N}\sum_m S_m \frac{d\Gamma}{d\nu}\big|_{\Delta\nu_m}$ and $\beta \equiv \frac{1}{2N}\sum_m S_m \frac{d^2\Gamma}{d\nu^2}\big|_{\Delta\nu_m}$, then

$$
\begin{aligned}
\sigma_\Gamma^2 &= \left\langle \delta\Gamma_{\text{tot}}^2 \right\rangle - \left\langle \delta\Gamma_{\text{tot}} \right\rangle^2 = \left\langle \left(\alpha\,\delta f + \beta\,\delta f^2\right)^2 \right\rangle - \left\langle \alpha\,\delta f + \beta\,\delta f^2 \right\rangle^2 \\
&= \alpha^2 \left\langle \delta f^2 \right\rangle + \beta^2 \left\langle \delta f^4 \right\rangle + 2\alpha\beta \left\langle \delta f^3 \right\rangle - \alpha^2 \left\langle \delta f \right\rangle^2 \\
&\quad - \beta^2 \left\langle \delta f^2 \right\rangle^2 - 2\alpha\beta \left\langle \delta f \right\rangle \left\langle \delta f^2 \right\rangle \\
&= \alpha^2 \sigma_{\delta f}^2 + \beta^2 \sigma_{\delta f^2}^2
\end{aligned}
\tag{16}
$$

In case of no PDH offset, $\alpha = 0$ and Eq. (16) becomes $\sigma_\Gamma = |\beta|\,\sigma_{\delta f^2}$. Notice that in the calculations, we exploited the fact that $\langle \delta f \rangle = 0$ and $\langle \delta f^3 \rangle = 0$ for symmetry. The relative noise of the cavity gain is simply given by

$$
\sigma_{\Gamma,\text{rel}} = \frac{\sigma_\Gamma}{\Gamma_{\text{tot}}}
\tag{17}
$$

Equivalently, the relative intracavity power noise is $\sigma_{P,\text{rel}} = \sigma_P/P_{\text{tot}}^{(\text{cav})} = \sigma_{\Gamma,\text{rel}}$.

Finding a simple relation between $\sigma_{\delta f}$ and $\sigma_{\delta f^2}$ is important, because we have direct access to the first quantity, but not to the second. This relation can be found for instance rewriting Eq. (16) in the case of Gaussian-distributed noise δf. For simplicity, we define $\delta f = x$ and $\delta f^2 = y = x^2$, so that the Gaussian distribution of δf can be written as

$$\int_{-\infty}^{\infty} \frac{1}{\sqrt{2\pi}\sigma_x} e^{-\frac{x^2}{2\sigma_x^2}} \, dx = \int_{0}^{\infty} \frac{2}{\sqrt{2\pi}\sigma_x} e^{-\frac{x^2}{2\sigma_x^2}} \, dx$$

$$= \int_{0}^{\infty} \frac{1}{\sqrt{2\pi}\sigma_x \sqrt{y}} e^{-\frac{y}{2\sigma_x^2}} \, dy \tag{18}$$

where we performed the substitution $y = x^2$, so that $dx = 1/2\sqrt{y} \, dy$. Notice that the domain of y is $\mathbb{R}^+$, so we exploited the symmetry of the Gaussian distribution of x to change the integration range from $(-\infty, +\infty)$ to $[0, +\infty)$. The distribution of the variable $y = \delta f^2$ is thus $\frac{1}{\sqrt{2\pi}\sigma_x \sqrt{y}} e^{-\frac{y}{2\sigma_x^2}}$. Its variance is by definition

$$\sigma_y^2 = \int_{0}^{\infty} \frac{1}{\sqrt{2\pi}\sigma_x \sqrt{y}} e^{-\frac{y}{2\sigma_x^2}} y^2 \, dy$$

$$- \left(\int_{0}^{\infty} \frac{1}{\sqrt{2\pi}\sigma_x \sqrt{y}} e^{-\frac{y}{2\sigma_x^2}} y \, dy \right)^2 = 2\sigma_x^4 \tag{19}$$

This result tells us that $\sigma_{\delta f^2} = \sqrt{2}\sigma_{\delta f}^2$, so Eq. (16) becomes

$$\sigma_\Gamma^2 = \alpha^2 \sigma_{\delta f}^2 + 2\beta^2 \sigma_{\delta f}^4 \tag{20}$$

Some important considerations can be done looking at our simple analytical model. First, we expect different behaviors for different values of the finesse, since it is directly related to the cavity linewidth as well as the gain function and its derivatives. In particular, we expect a higher sensitivity to the suppression effect for higher finesse. The same holds for the width of the laser spectrum, since for a wider spectrum, more external teeth with a wider detuning are involved, contributing to the noise suppression.

In the next sections, we will show that it is possible to apply the discussed theory to obtain a strong suppression of the intensity noise, given a specific enhancement cavity gain, though some experimental limitations occur. As it will be extensively explained, this can be obtained exploiting the relative offset f_0 of the combs, together with a proper choice of different enhancement cavity finesse values.

3 Simulations

The cavity-laser system has been simulated to comprehend the impact of f_0 (thus of f_{ceo}) on the total gain, on its relative noise, and on the peak power of the stored pulses. Notice that, since we showed $\sigma_{P,rel} = \sigma_{\Gamma,rel}$, from now we will refer to it as a unique σ_{rel}. These simulations allow estimating the effective cost paid in terms of gain reduction to have a strong noise suppression. All the calculations have been performed with Wolfram Mathematica and Matlab. We took the experimental data as technical parameters for the simulations (see

Sect. 4), in particular, we set the repetition rate of the laser to $f_{rep} = 100$ MHz. To simulate the spectrum shape $S(\nu)$, we used a supergaussian function of the 4th order of the form $S(\nu) \propto \exp\left[-\ln 2 \left(2 \left(\nu - \nu_0\right)/\Delta\nu\right)^8\right]$, where the FWHM $\Delta\nu$ is given by $\Delta\nu = -c/\lambda_0^2 \Delta\lambda$, and $\nu_0 = c/\lambda_0$, being $\Delta\lambda = 2.7$ nm the corresponding FWHM in the wavelength domain, and $\lambda_0 = 1035$ nm the central wavelength. As far as the cavity is concerned, we simulated a 4-mirrors crossed cavity in overcoupled configuration, switching between the two different values of the finesse of 4300 and 1800. We set the offset of the PDH error signal to 0, assuming a perfect locking of mode m_0. Nevertheless, values of f_{pdh} up to some kHz do not affect the results appreciably. Then, we took $\sigma_{\delta f} = 5$ kHz, which is the value we experimentally measured. Finally, we assumed δf Gaussian distributed, so we estimated σ_{rel} from Eq. (20).

Figure 3 shows the results of the simulations of normalized Γ_{tot}, σ_{rel}, and P_{peak} as functions of f_0, for a cavity of finesse 4300. We chose a normalized plot to highlight the different trends of the traces. Notice that the peak power has been calculated from the laser spectrum, taking into account the cavity spectral filter effect and mode-dependent phase. After multiplying all these terms, an Inverse Fourier Transform allows estimating the shape of the resulting pulses inside the cavity in temporal domain, thus P_{peak}. As it can be easily noticed, all simulated quantities decrease when the laser-cavity offset f_0 rises. Nevertheless, there is a faster drop in terms of relative noise with respect to the other traces. For example, in the first 10 MHz, the normalized amplitude of the noise reduces to 0.27, while the peak power remains around 0.70, and the total gain (average
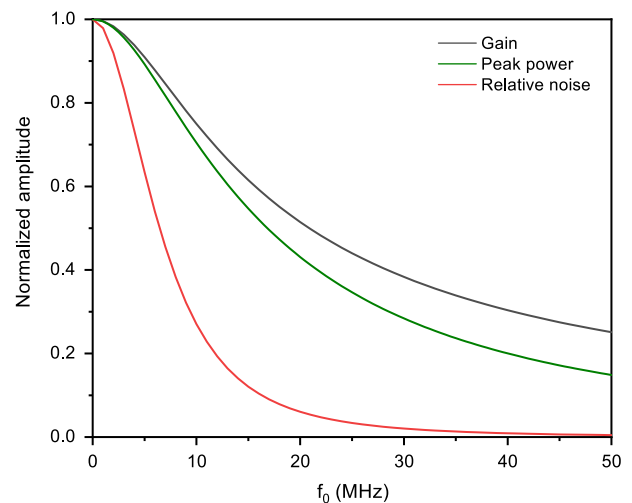

Fig. 3 From top to bottom: gain (black), stored pulses peak power (green), and relative power noise σ_{rel} (red) as functions of the relative frequency offset f_0. Traces are normalized to their respective values in $f_0 = 0$. Here the finesse is 4300
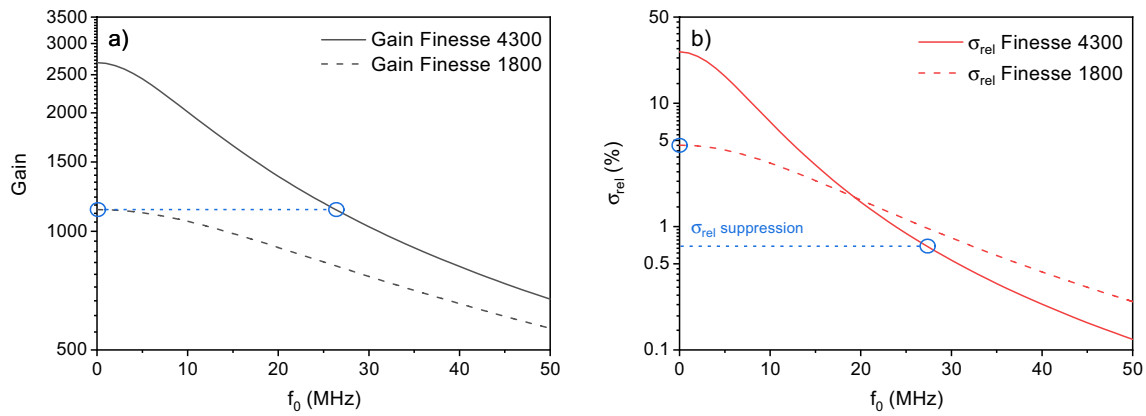
Fig. 4 Gain (**a**) and relative intensity noise σ_{rel} (**b**) in logarithmic scale for finesse values $F = 4300$ and $F = 1800$. For both configurations, the PDH offset is zero and the frequency noise is $\sigma_{\delta f} = 5$ kHz. The blue line in panel a) indicates the higher gain value possible for

$F = 1800$ at a relative frequency offset $f_0 = 0$, namely gain 1130. The same gain is reached for finesse 4300 at $f_0 = 30$ MHz. In panel **b**, we show the suppression of σ_{rel} between the two configurations highlighted in panel **a**

intracavity power) stays at about 0.75. Thus, in general, there is always an advantage in terms of signal-to-noise ratio for both P_{peak} and P_{cav}, leaving the point $f_0 = 0$. This general behavior has immediate repercussions in all those applications of non-linear optics such as the generation of high order harmonics (HHG) and ICS X-ray generation. In HHG, a slight noise reduction in the fundamental harmonic can lead to a substantial suppression for HHG noise, by an amount proportional to the order of the generation process. Since the framework in which this work has been developed is the study and realization of optical cavities for ICS X-rays generation, we will concentrate only on the cavity gain and its noise, omitting further considerations on P_{peak}. Indeed, in ICS experiments, scattering efficiency is more sensitive to average power variations than to intracavity pulses temporal broadening [22]. As a second simulation, we compared the behaviors of two cavities with different values of finesse. In particular, we calculated total gain and relative noise for finesse values of 4300 and 1800, and the results are reported in Fig. 4. In panel a, we report Γ_{tot}, while in panel b) σ_{rel}, for a cavity with finesse values of 4300 and 1800. The gain decreases similarly for the two cases, although the maximum gain is a function of the finesse. We start from a gain of 2680 for $F = 4300$, and of 1130 for $F = 1800$. The noise at zero offset is different for the two cases, too, being 26.2% and 4.6%, respectively. For both finesse values, the gain decreases slower than the noise. From these simulations, we demonstrated that, given a certain target gain, the noise can be reduced by setting a finesse higher than needed, and then increasing f_0 until the desired gain is reached, having a relative noise lower than the standard configuration of $f_0 = 0$. For example, in this case, the gain of 1130 can be conveniently reached starting from $F = 4300$ and increasing f_0 until $\Gamma_{tot} = 1130$ is reached (approximately $f_0 = 27$

MHz, instead of choosing a finesse of 1800 and couple it to the laser with $f_0 = 0$. In this way, the same gain is achieved with a noise reduction of a factor 6.4 (0.72% against 4.6%).

4 Experiment

In this section, we report on the experiment we performed to study and prove the f_0-dependent noise suppression. The experimental setup is schematized in Fig. 5. The laser source is an Orange Yb:fiber mode-locked oscillator from Menlo Systems, with a repetition rate of 100 MHz, and a bandwidth of 20 nm, centered at 1035 nm. A BK7 window (with a thickness of 5 mm) is inserted in the laser cavity, to control f_{ceo} by a manual micrometric rotation stage (labelled RS in the schematics). The laser output power is on the order of 200 mW. The output pulses pass through a NewFocus Wideband 4004 IR Electro-Optic Modulator (EOM), that introduces a frequency modulation at 3.5 MHz, needed for the Pound-Drever-Hall (PDH) cavity-laser stabilization. Though not strictly required for this experiment (but already integrated in our experimental setup), an optical amplification stage follows. The laser beam is stretched in time and selected in frequency domain by an Optigrate BG Pulse Chirped Volume Bragg Grating (CVBG) and power-enhanced by a 4 m long Yb-fiber amplifier (based on Liekki Yb1200-12/125DC-PM), pumped by a multimode 976 nm laser diode (Photontec M976). The CVBG is required to avoid nonlinear effects inside the amplifier's fiber. Here, the pulse length is stretched from 200 fs to 380 ps, while the spectrum is reduced to a FWHM of 2.7 nm, with a shape well described by the 4th-order supergaussian function used in the simulations. The output power from the amplifier has been set to 1.1 W. Then the pulses go
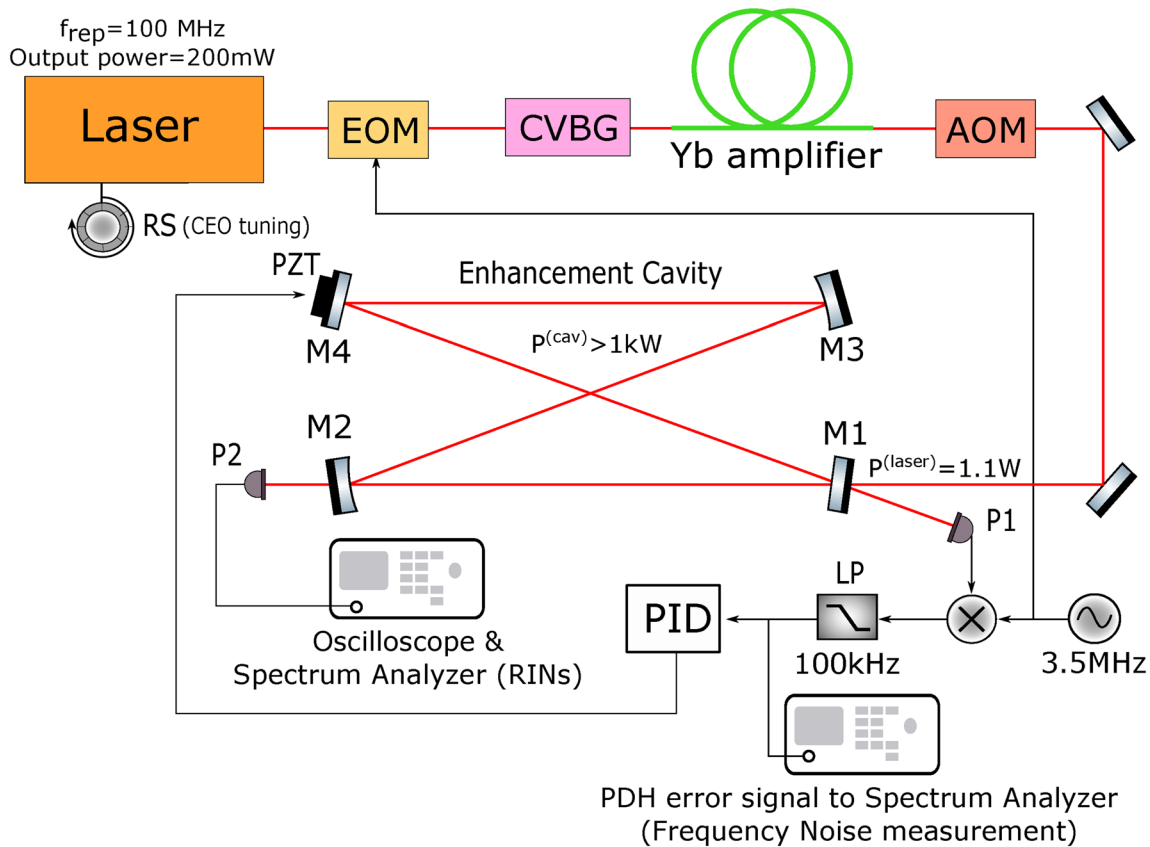
Fig. 5 Scheme of the setup used for our experiment. The source laser is represented in orange. *RS* micrometric rotation stage, *EOM* Electro-Optic modulator, *CVBG* Chirped Volume Bragg Grating, *AOM* Acousto-optical modulator, *M1, M2, M3, M4* enhancement cavity mirrors, *P1* and *P2* photodetectors, *LP* 100 kHz 5th-order low-pass filter, *PZT* piezoelectric actuator

through a NEOS Acousto-optical Modulator (AOM), necessary for the measurement of the cavity finesse exploiting the modulation technique described in [23]. At this point, the laser is coupled with a four-mirror crossed ring enhancement cavity. The four mirrors by Layertec have a negligible dispersion (single mirror Group Delay Dispersion $GDD_{mirror} = 6.7$ fs^2) in the spectral region of interest. M1 and M4 are flat, while M2 and M3 are curved, with a radius of curvature of 750 mm. Also, the air dispersion inside the cavity is negligible ($GDD_{air} = 48.8$ fs^2) in our experimental setup. Since our cavity is overcoupled, we exploited two different input couplers M1 to switch between two different finesse values. One input coupler has a power reflectivity of $R = 99.66\%$ and gives a finesse 1800 (measured 1785 ± 50, $\Gamma_{tot} = 1137 \pm 30$), while the other has $R = 99.86\%$ and gives a finesse of 4300 (measured 4270 ± 110, $\Gamma_{tot} = 2720 \pm 70$). All the other mirrors have a high reflectivity ($R > 0.99999$). The Free Spectral Range of the cavity is controlled by a piezoelectric actuator (PZT) attached to the mirror M4. The active stabilization of the cavity against the laser is based on the PDH error signal generated from the beam reflected from M1. It is detected by the photodetector P1 (Fermionics

Opto-Technology FD500W), and low-pass filtered at 100 kHz to cancel the high-frequency components. The PDH error signal is then sent to a PID controller, which elaborates the signal and applies it to the PZT. The transmitted signal is measured by the photodiode P2 (Thorlabs PBD150A, bandwidth 5 MHz) behind M2.

We measured the Relative Intensity Noise (RIN) of the laser before coupling to the cavity, showing the results in the left panel of Fig. 6. The measurement has been performed using a large bandwidth photodetector and an Agilent E4445A Spectrum Analyzer, high-pass filtered at approximately 150 Hz to remove the DC component. The high-pass (HP) filter response has been removed to estimate the integrated noises. Then, the relative integrated noise from 1 Hz to 1 MHz of the laser is $\sigma_{rel} = 0.03\%$. The RIN background coincides with the photodiode floor. For what concerns the RIN behavior, we observe a decreasing curve on the whole band (except for the region influenced by the filter). The higher average level approaches -90 dB Hz^{-1}, except for a -80 dB Hz^{-1} noise peak, while the minimum approached at 1 MHz is below -130 dB Hz^{-1}. Several peaks are noticeable in the intensity noise spectrum, in particular between
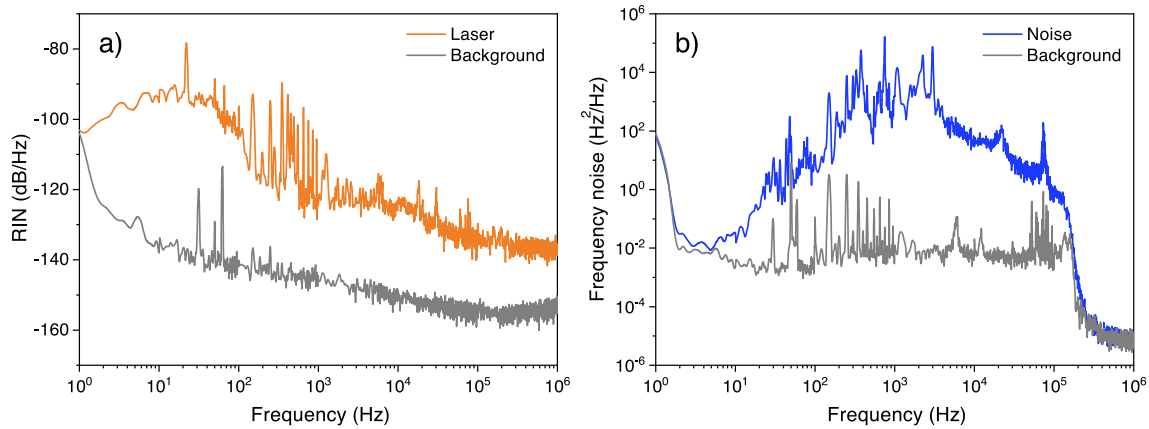
Fig. 6 **a** RIN of the laser before coupling to the cavity. **b** Frequency noise of the laser-cavity coupled system

100 Hz and 2 kHz. Those are due to the amplifier pump diode's electrical noise, which is directly transferred to the amplified signal, although it is cut at approximately 1 kHz by Ytterbium spontaneous decay [24].

At this point, we coupled the laser to the cavity (in this case $F = 4300$), and we measured the frequency noise of the coupled system, shown in panel b of Fig. 6. This measurement has been performed by acquiring the PDH error signal after LP, and converting it into a detuning signal by the so-called discriminator constant k_d [4], defined as $k_d = \frac{\delta \nu}{\delta V}$, where $\delta \nu$ is a detuning variation between the laser and the cavity frequencies, while δV is the corresponding variation on the PDH signal. We have $k_d = 1.56 \times 10^5$ Hz V^{-1}. Here, the background corresponds to the frequency noise measured with the cavity out of resonance. To better estimate the noise without feedback contributions, such measurement has been performed with a weak lock (feedback bandwidth approximately 1 kHz). The low-frequency peaks are mainly due to mechanical vibrations. On the other hand, the noise around 10 kHz comes from the piezoelectric actuator resonance. Other contributions derives from the laser frequency noise spectrum but are not distinguishable from the cavity ones, since the discriminator measures only relative detunings. The highest frequency noise level is reached by mechanical contributions, and it is approximately 10^3–10^4 Hz^2 Hz^{-1}. The sharp cut at 100 kHz is due to the LP filter of the PDH stabilization. From the PSD of panel b of Fig. 6 we calculated the experimental integrated frequency noise $\sigma_{\delta f} = 5063$ Hz, by taking the square root of PSD integral (calculated between 1 Hz and 1 MHz).

Exploiting the setup described above, we compared the Relative Intensity Noise of the signal transmitted from the mirror M2 with the two available finesse values and different f_0, bearing in mind that such signal is directly proportional to the intracavity power. In addition, we acquired temporal

traces of the transmitted beam to have a better visualization of the results.

As mentioned at the beginning of this Section, the control of f_0 is allowed by the presence of a BK7 window inside the laser cavity. The window can rotate at different angles with respect to the beam, thus modifying the intracavity dispersion, and inducing a f_{ceo} change. As explained in Refs. [25, 26], when f_0 is minimized, only one transmission peak is maximized in a cavity scan. On the contrary, when $f_0 = f_{rep}/2$ two consecutive peaks have the same intensity, visibly lower than the maximum of the previous situation. We experimentally found these points (see Fig. 7) by adjusting the BK7 window angle, so calibrating the control of f_0.

Indeed, from simple goniometric considerations, f_0 can be written as a function of the window angle θ

$$f_0(\theta) = \frac{f_{rep}/2}{-\frac{1}{\sqrt{1-k^2 \sin^2 \theta_0}} + \frac{1}{\sqrt{1-k^2 \sin^2 \theta_{max}}}} \left(\frac{1}{\sqrt{1 - k^2 \sin^2 \theta}} - \frac{1}{\sqrt{1 - k^2 \sin^2 \theta_0}} \right)$$

(21)

where θ_0 and θ_{max} are the angular positions of $f_0 = 0$ and $f_0 = f_{rep}/2$, respectively, taking the perpendicular position of the window as $\theta = 0$, while $k = n_{air}/n_{BK7} = 1/1.507$ at 1035 nm. Estimating the uncertainties on the rotation stage and possible mount hysteresis, we claim an error of ± 5 MHz on our f_0 measurements.

To investigate the noise transfer from the frequency detuning to the stored power, we acquired different RIN traces, shown in Fig. 8. Here, a comparison between the transmitted power RIN for finesse 1800 and for finesse 4300 in both cases with $f_0 = 0$ and $f_0 = 45$ MHz is shown (curves
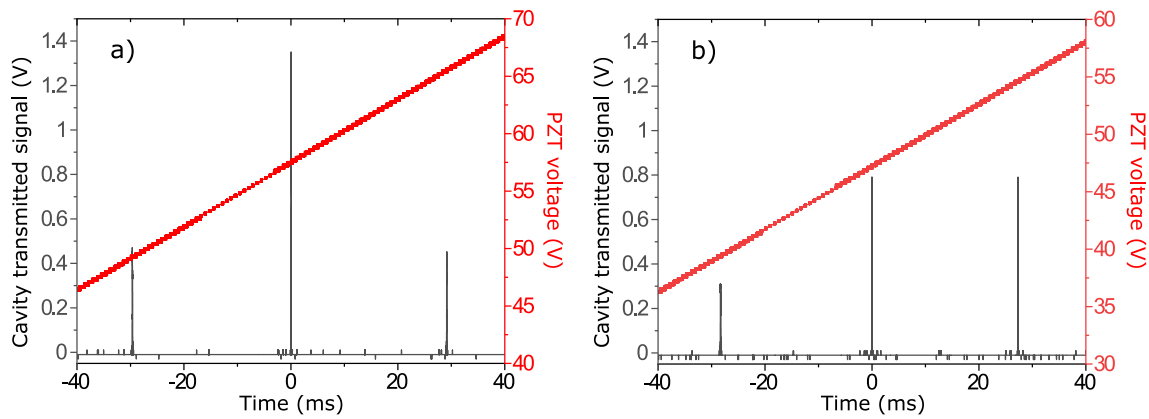
Fig. 7 Resonance peaks (black) and voltage applied to the piezoelectric actuator (red) during a scan of the cavity length. The distance between two peaks is equal to a variation of the cavity length, corresponding to a FSR. In panel **a**, f_0 is null, thus the secondary peaks around the central one are symmetric and considerably lower than it. In panel **b**, the opposite situation is shown: $f_0 = f_{rep}/2 = 50$ MHz, so the primary peak and its neighbor on the right have the same intensity and symmetry of secondary peaks is broken

Fig. 8 RIN traces acquired from photodetector P2 in cavity locking condition. From top to bottom (labeled in the legend both in colors and letters) traces acquired for: **a** $F = 4300$ and $f_0 = 0$, **b** $F = 1800$ and $f_0 = 0$, **c** $F = 4300$ and $f_0 = 45$ MHz, **d** $F = 1800$ and $f_0 = 45$ MHz, **e*** $F = 4300$ and $f_0 = 45$ MHz with PID parameters optimized for this case, and **f** input laser RIN baseline. Except for data (**e**, **f**), all the traces have been measured by leaving the PID cavity-lock parameters unaltered. The highlighted traces (**b**, **c**, **e**) correspond to the same gain factor $\Gamma_{tot} = 1137 \pm 30$
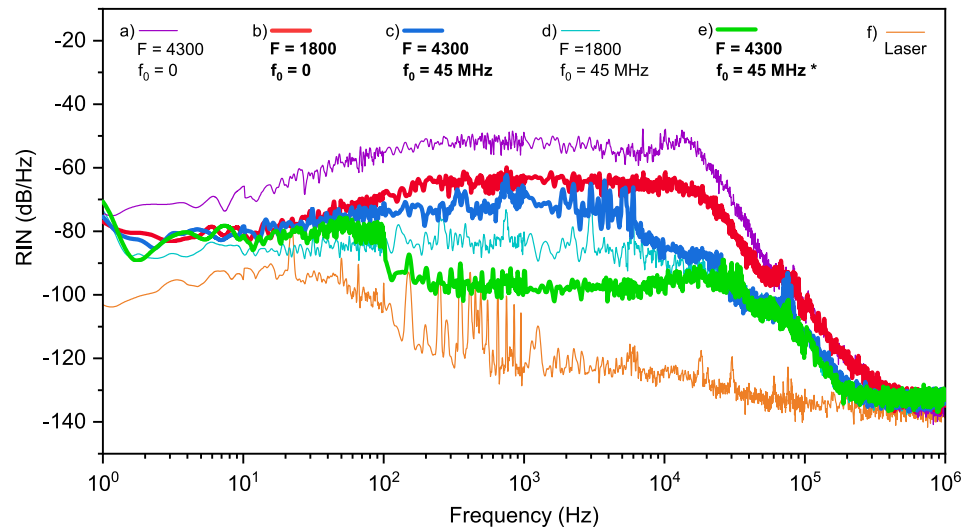
from (a) to (d)). As a reference baseline for these measurements, we report the laser RIN in orange (f).

The choice of $f_0 = 45$ MHz is not accidental, but we experimentally set it to the value such that the configuration with $F = 4300$ and $f_0 = 45$ MHz has the same gain as the configuration with $F = 1800$ and $f_0 = 0$. Indeed, we measured the same cavity passive gain comparing the transmission power levels for finesse 1800, $f_0 = 0$ and finesse 4300, $f_0 = 45$ MHz, so having the occasion to directly compare the contribution of f_0 on noise suppression. It is worth noting that we fixed the PID lock parameters (chosen by optimizing the cavity lock for finesse 1800, $f_0 = 0$) to compare different finesse values and offsets without changing the loop gain or bandwidth. As a last step, we acquired also a RIN of the transmitted signal with finesse 4300 and $f_0 = 45$ MHz optimizing the feedback parameters (trace

(e)). This latter measurement shows a further enhancement in terms of power fluctuations. The higher trace, namely the one labeled (a), is the one of finesse 4300 and $f_0 = 0$. Before 10 kHz it is constant at about -50 dB Hz^{-1}, while a broad peak at 11 kHz appears at the piezoelectric actuator resonance. After the resonance, the trace falls and reaches the background floor around 400 kHz. The same drop is noticeable in trace (b), which is the RIN of finesse 1800 and $f_0 = 0$. On the other hand, the average is 20 dB lower than the previous, and no piezoelectric actuator resonances are visible. A substantial change is noticeable looking at trace (c), acquired for finesse 4300 but high f_0. Though, the gain is the same for this curve and (b), while the noise is on average 10 dB lower between 100 Hz and 10 kHz, and 20 dB lower between 10 and 50 kHz. Furthermore, the noise fall reaches the floor at 200 kHz instead of 400 kHz. A similar

behavior can be encountered for trace (d), namely the one obtained from finesse 1800 and $f_0 = 45$ MHz (with a lower average of about 10 dB before 10 kHz). A difference in the RIN fall around 10 kHz of the two curves (a) and (b) and the three curves (c), (d), and (e) can be observed. We attribute it to the general noise reduction in presence or absence of f_0, thus a rescaling of the RIN level also for frequencies above the PID bandwidth. The best noise suppression case is then represented in trace (e), where we combined the effect of f_0 with an optimization of the feedback parameters. The feedback noise reduction is evident between 100 Hz and 10 kHz (which is the feedback bandwidth, i.e., the actuator mechanical resonance frequency), where the noise remains on average below -90 dB Hz^{-1}.

From the RINs, we calculated the relative noise integrating from 1 Hz to 1 MHz obtaining the following values: $\sigma_a = 32.5\%$, $\sigma_b = 8.0\%$, $\sigma_c = 2.5\%$, $\sigma_d = 1.2\%$, and $\sigma_e = 0.4\%$. Sigmas are labeled with the same letter of the correspondent RIN. Notice that there is agreement between the simulated noise decreasing trend and the experimental values.

The core of this work resides in the difference between σ_b and σ_c. Indeed, these measurements have been obtained at the same gain (thus at the same cavity stored power), but the power fluctuations are lowered by f_0 of a factor 3.2. Of course, the compensation becomes more evident after the PID optimization, which leads to an integrated relative noise reduced of a factor 20 with respect to the one from trace (b).

For a better visualization of the results, we report the three cases of interest (b), (c), and (e) transmission power traces in Fig. 9.

All the represented measures were acquired by the same detector used for the RINs and sent to the oscilloscope. The color used in the picture recalls the correspondent cases in Fig. 8. Thus, from left to the right, we encounter cases (b), (c), and (e). As expected, the relative noise is subjected to a drop as f_0 increases, passing from $\sigma_b = 8.0\%$ for $F = 1800$ and $f_0 = 0$, to $\sigma_e = 0.4\%$ for $F = 4300$ and $f_0 = 45$ MHz and optimized feedback, while maintaining the same gain. Notice that even though the order of magnitude of the relative noises is the same of simulation (as well as their drop at increasing f_0), the measured values are lower than the predicted ones in most of the cases. This fact can be ascribed to a partial suppression given by the PDH feedback, as can be seen from the RIN traces.

A final comment should be addressed to the comparison between the simulations and the experimental data. The value of f_0 at which the two configurations have the same gain is different between the simulations and the experiment (30 MHz versus 45 MHz, respectively). The reasons could be manifold: the gain function Γ in Eq. (13) has been expanded up to the second order, together with an
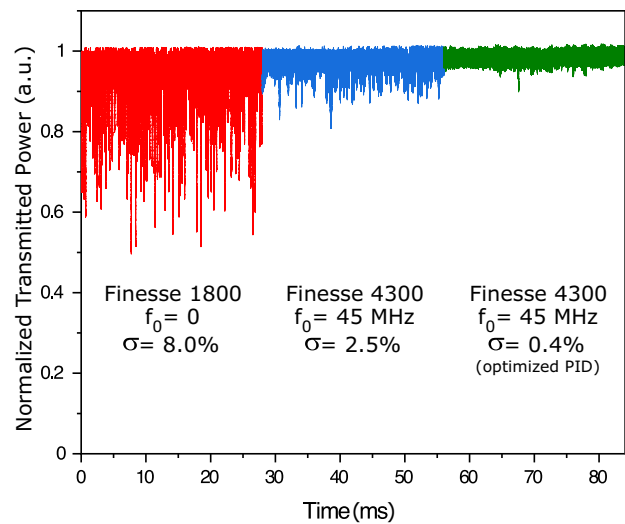

Fig. 9 Time domain traces of finesse 1800-$f_0 = 0$ (red, left), finesse 4300-$f_0 = 45$ MHz before (blue, central) and after (green, right) the PID optimization. Cavity gain (thus stored power) is essentially the same in all represented cases. The traces have been merged in a unique time axis for simplicity of representation

approximated modelling of the laser spectrum and experimental uncertainties on the f_0 measurement.

5 Conclusions

In conclusion, we demonstrated both theoretically and experimentally the suppression effect of f_0 (thus of f_{ceo}) over the frequency noise contribution to power fluctuations of a laser-cavity locked system. We showed that increasing f_0 leads to a substantial noise reduction, visible both in terms of integrated relative noise and its spectrum. We also demonstrated that the enhancement cavity gain decreases slower than the noise. This finding opens the possibility of exploiting higher finesse to obtain a desired cavity gain (average stored power), while maintaining substantially lower power instabilities. In particular, we experimentally showed that a cavity gain of approximately $\Gamma_{tot} = 1130$ can be obtained either with a finesse of 1800 and an offset $f_0 = 0$, or with a finesse of 4300 and an offset $f_0 = 45$ MHz. However, the relative noise in these two cases is very different, passing from 8.0 to 2.5%, respectively. In the last configuration, an optimization of the PID parameters allowed us to further decrease the relative noise to 0.4%.

References

1. A.S. Villar, Am. J. Phys. **10**, 922 (2008). https://doi.org/10.1119/1.2937903
2. J. Morville, D. Romanini, M. Chenevier, A. Kachanov, Appl. Opt. **41**(33), 6980 (2002)
3. L.S. Ma, J. Ye, P. Dubé, J.L. Hall, J. Opt. Soc. Am. B **16**(12), 2255 (1999)
4. D. Gatti, R. Gotti, T. Sala, N. Coluccelli, M. Belmonte, M. Prevedelli, P. Laporta, M. Marangoni, Opt. Lett. **40**(22), 5176 (2015)
5. G. Berden, R. Peeters, G. Meijer, Int. Rev. Phys. Chem. **19**(4), 565 (2000). https://doi.org/10.1080/014423500750040627
6. D.A. Long, A.J. Fleisher, S. Wojtewicz, J.T. Hodges, Appl. Phys. B **115**, 149 (2014)
7. F. Adler, M.J. Thorpe, K.C. Cossel, J. Ye, Annu. Rev. Anal. Chem. **3**(1), 175 (2010). https://doi.org/10.1146/annurev-anchem-060908-155248
8. B. Bernhardt, A. Ozawa, P. Jacquet, M. Jacquey, Y. Kobayashi, T. Udem, R. Holzwarth, G. Guelachvili, T.W. Hänsch, N. Picqué, Nat. Photon. **1**, 55 (2010). https://doi.org/10.1038/nphoton.2009.217
9. N. Hoghooghi, R.J. Wright, A.S. Makowiecki, W.C. Swann, E.M. Waxman, I. Coddington, G.B. Rieker, Optica **6**(1), 28 (2019)
10. R.J. Jones, K.D. Moll, M.J. Thorpe, J. Ye, Phys. Rev. Lett. **94**, 193201 (2005). https://doi.org/10.1103/PhysRevLett.94.193201
11. C. Gohle, T. Udem, M. Herrmann, J. Rauschenberger, R. Holzwarth, H.A. Schuessler, F. Krausz, T.W. Hänsch, Nature **7048**, 234 (2005). https://doi.org/10.1038/nature03851
12. T.K. Allison, A. Cingöz, D.C. Yost, J. Ye, Phys. Rev. Lett. **107**, 183903 (2011). https://doi.org/10.1103/PhysRevLett.107.183903
13. P. Cardarelli, A. Bacci, R. Calandrino, F. Canella, R. Castriconi, S. Cialdi, A. Del Vecchio, F. di Franco, I. Drebot, M. Gambaccini, D. Giannotti, A. Loria, G. Mettivier, G. Paternò, V. Petrillo, M. Rossetti Conti, P. Russo, A. Sarno, E. Suerra, A. Taibi, L. Serafini, Phys. Med. **77**(February), 127 (2020). https://doi.org/10.1016/j.ejmp.2020.08.013
14. H. Telle, G. Steinmeyer, A. Dunlop, J. Stenger, D. Sutter, U. Keller, Appl. Phys. B **4**, 327 (1999). https://doi.org/10.1007/s003400050813
15. F. Helbing, G. Steinmeyer, U. Keller, IEEE J. Sel. Top. Quantum Electron. **9**(4), 1030 (2003). https://doi.org/10.1109/JSTQE.2003.819104
16. A. Ashkin, G. Boyd, J. Dziedzic, IEEE J. Quantum Electron. **2**(6), 109 (1966). https://doi.org/10.1109/JQE.1966.1074007
17. O. Svelto, *Principles of Lasers* (Spinger, Berlin, 2010)
18. M. Durand, Y. Wang, J. Lawall, Appl. Phys. B **108**(4), 749 (2012). https://doi.org/10.1007/s00340-012-5147-x
19. J. Petersen, A. Luiten, Opt. Express **11**(22), 2975 (2003). https://doi.org/10.1364/OE.11.002975https://opg.optica.org/oe/abstract.cfm?uri=oe-11-22-2975
20. R.W.P. Drever, J.L. Hall, F.V. Kowalski, J. Hough, G.M. Ford, A.J. Munley, H. Ward, Appl. Phys. B Photophys. Laser Chem. **2**, 97 (1983). https://doi.org/10.1007/BF00702605
21. N. Coluccelli, M. Cassinerio, A. Gambetta, P. Laporta, G. Galzerano, Sci. Rep. **1**, 16338 (2015). https://doi.org/10.1038/srep16338
22. A. Variola, F. Zomer, E. Bulyak, P. Gladkikh, V. Skomorokhov, T. Omori, J. Urakawa, Phys. Rev. ST Accel. Beams **14**, 031001 (2011). https://doi.org/10.1103/PhysRevSTAB.14.031001
23. G. Galzerano, E. Suerra, D. Giannotti, F. Canella, E. Vicentini, S. Cialdi, IEEE Trans. Instrum. Meas. **69**(11), 9119 (2020). https://doi.org/10.1109/TIM.2020.3001369
24. R. Paschotta, J. Nilsson, A. Tropper, D. Hanna, IEEE J. Quantum Electron. **33**(7), 1049 (1997). https://doi.org/10.1109/3.594865
25. G. Gagliardi, H.P. Loock, *Cavity-Enhanced Spectroscopy and Sensing Springer Series in Optical Sciences* (Springer, Berlin, 2014). https://doi.org/10.1007/978-3-642-40003-2
26. R.J. Jones, J. Ye, Opt. Lett. **2**, 1848 (2002). https://doi.org/10.1364/OL.27.001848